Supporting Information for **Investigation of micro-mechanical behavior and voiding of poly(ethylene-terephthalate)/poly(ethylene-*stat*-methyl acrylate) blends during tensile deformation**

Bongjoon Lee[†], Sebla Onbulak[‡], Yuewen Xu[§§], Vasily Topolkaraev[§], Ryan McEneany[§§], Frank Bates[†*], Marc Hillmyer[‡*]

[†]Department of Chemical Engineering and Materials Science, Minneapolis, MN 55455-0431

[‡]Department of Chemistry, University of Minnesota, Minneapolis, MN 55455-0431

[§]Corporate Research & Engineering, Kimberly-Clark Corporation, Neenah, WI 54957, USA

[§§] Void Technologies Inc., Neenah, WI

*Corresponding author (e-mail: bates001@umn.edu; hillmyer@umn.edu)

Supporting information

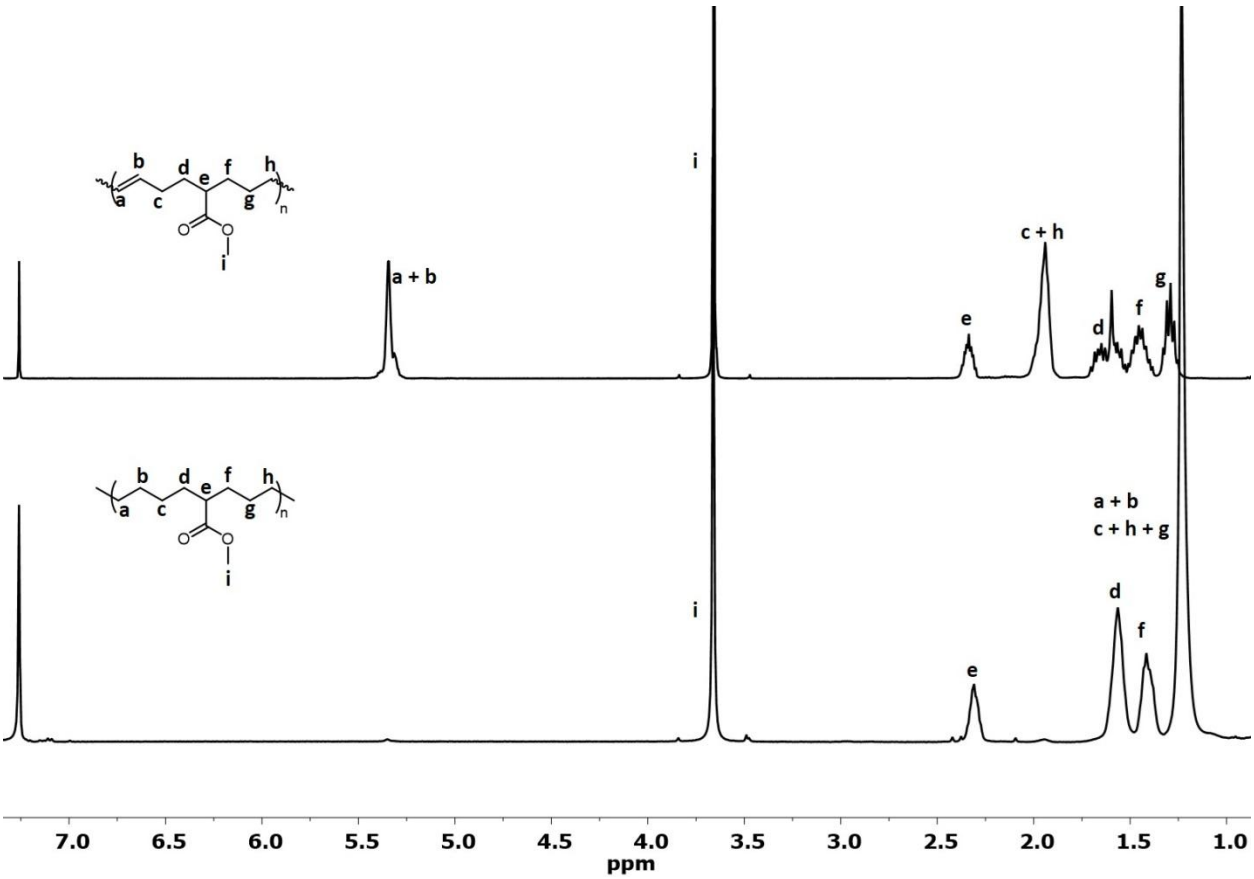

Figure S1. ^{1}H NMR spectra of PMEC (top) and PMA (bottom) in $CDCl_3$ at 25 °C.

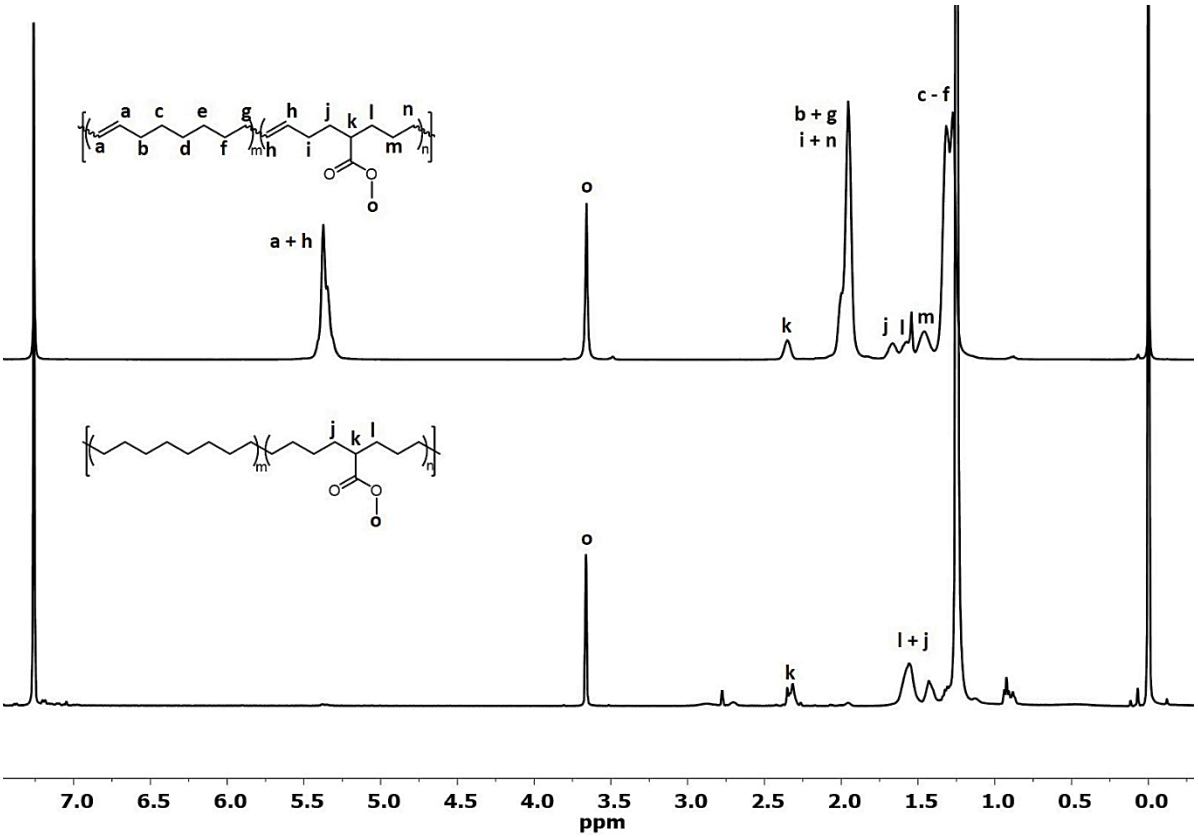

Figure S2. ^{1}H NMR spectra of P(COE$_{80}$-*s*-MEC$_{20}$) (top) and P(E$_{80}$-*s*-MA$_{20}$) (bottom) in $CDCl_3$ at 25 °C.

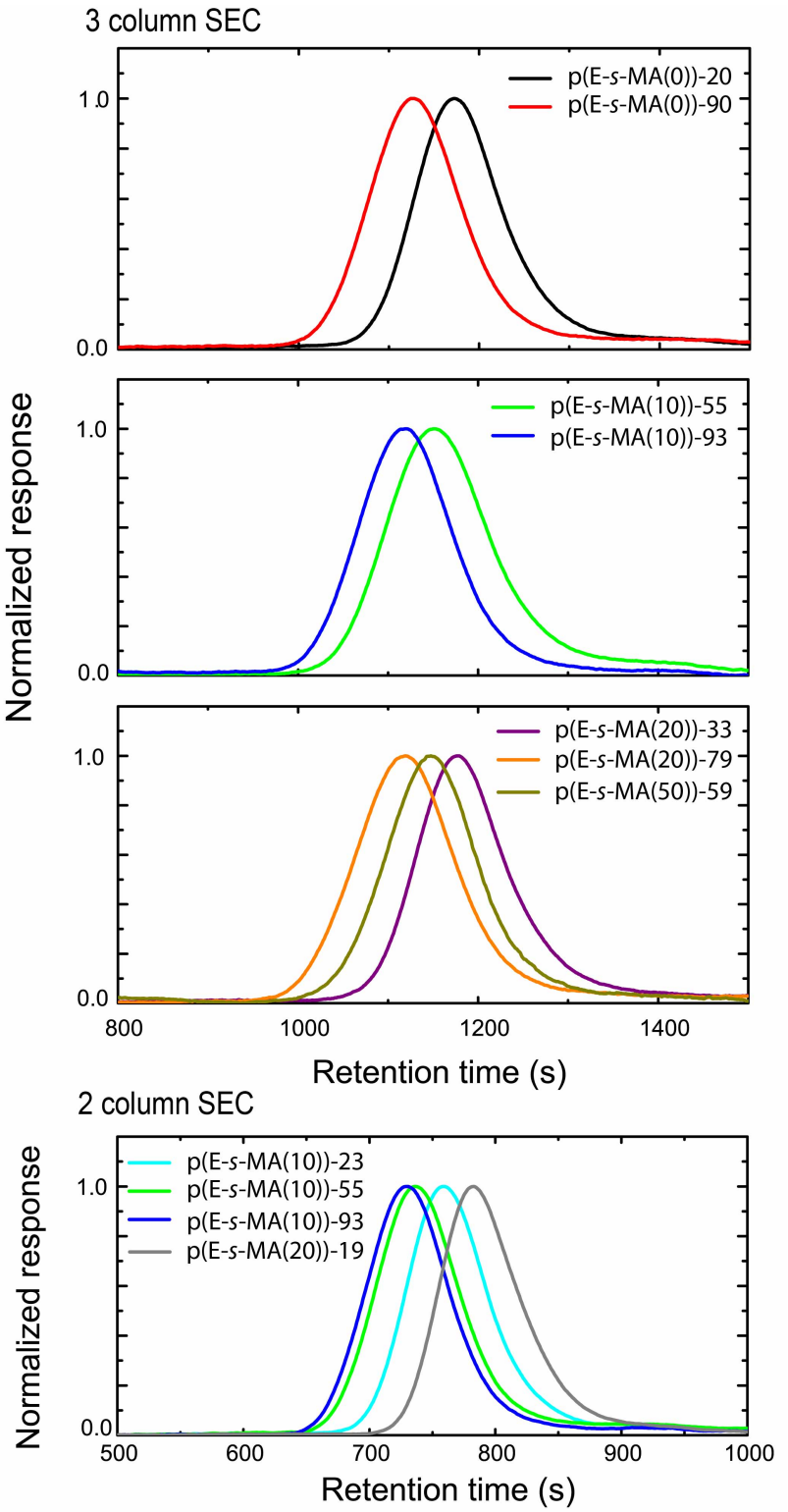

Figure S3. SEC traces of p(E-*s*-MA) series measured at 135 °C with 1,2,4-trichlorobenzene as the eluent at a flow rate of 1.0 mL min^{-1}. The SEC traces are measured by Polymer Laboratories GPC-220 liquid chromatograph fitted with three or two PlGel 10 μm Mixed-B columns and equipped with a refractometer.

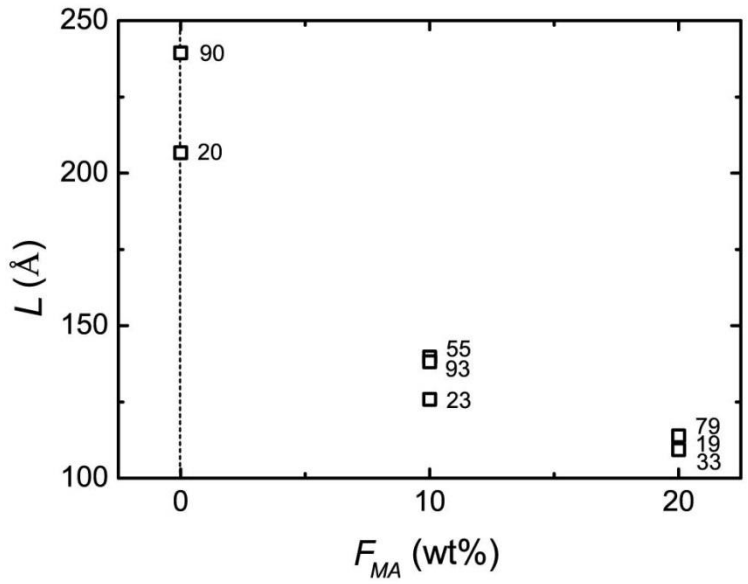

Figure S4. The long spacing (*L*) of lamellae stacking of p(E-*s*-MA) determined by SAXS.

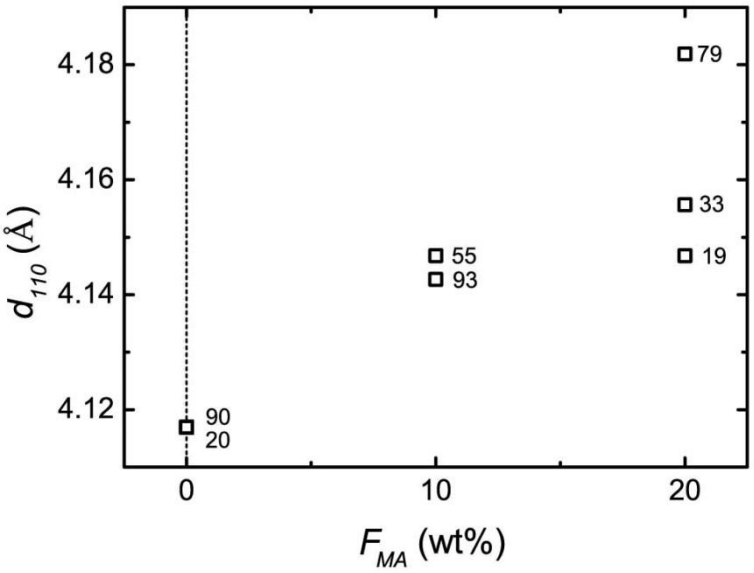

Figure S5. The spacing of (110) plane of orthorhombic PE crystal of p(E-*s*-MA) determined by WAXS.

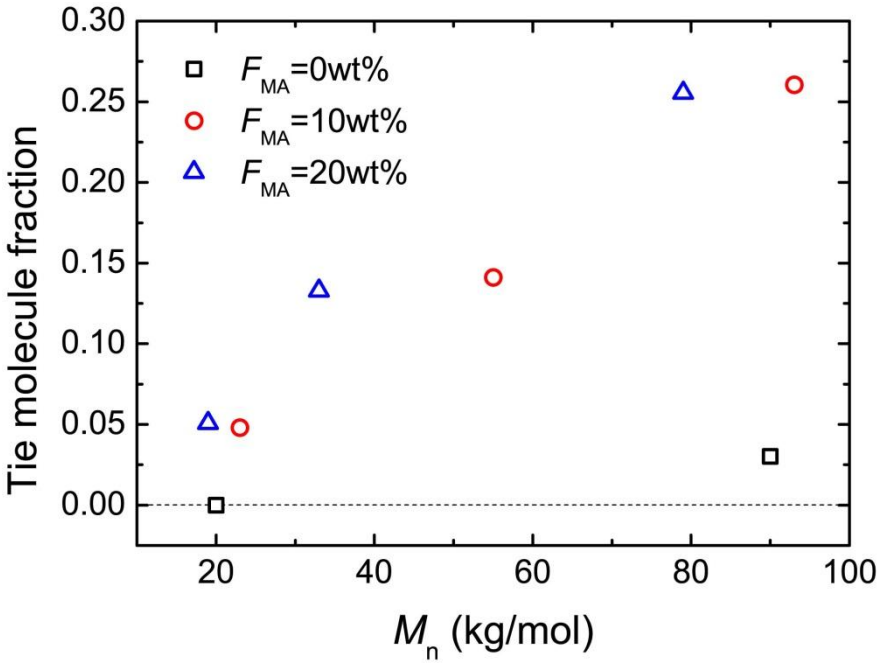

Figure S6 Calculated tie molecule fraction of p(E-*s*-MA) copolymer following Huang and Brown's procedure.[1]

Following Huang and Brown's approach, tie molecules will form if the end-to-end distance of a molecule in the melt is longer than the distance between the adjoining crystals. The root-mean square value $\underline{r}$ of the end to end distance of a random coil is given by

$$\underline{r} = (Dn'l^2)^{1/2} \tag{2}$$

Where $D = 6.8$ for PE, and the link length, $l = 0.153$nm.[1] n' is the number of links. The probability of a given end to end distance, r, is

$$p(r) = ar^2 \; exp \; exp \; (-b^2r^2) \tag{3}$$

a is constant and $b^2 = 3/2\underline{r}^2$.

It is assumed that tie molecule will form if the end-to-end distance of the random coil in melt is greater than $(2L_c + L_a)$. The probability of forming tie molecule is given below

$$P = \frac{1}{3}\frac{\int_{2L_c+L_a}^{\infty} r^2 \; exp \; exp \; (-b^2r^2) \; dr}{\int_0^{\infty} r^2 \; exp \; exp \; (-b^2r^2) \; dr} \tag{4}$$

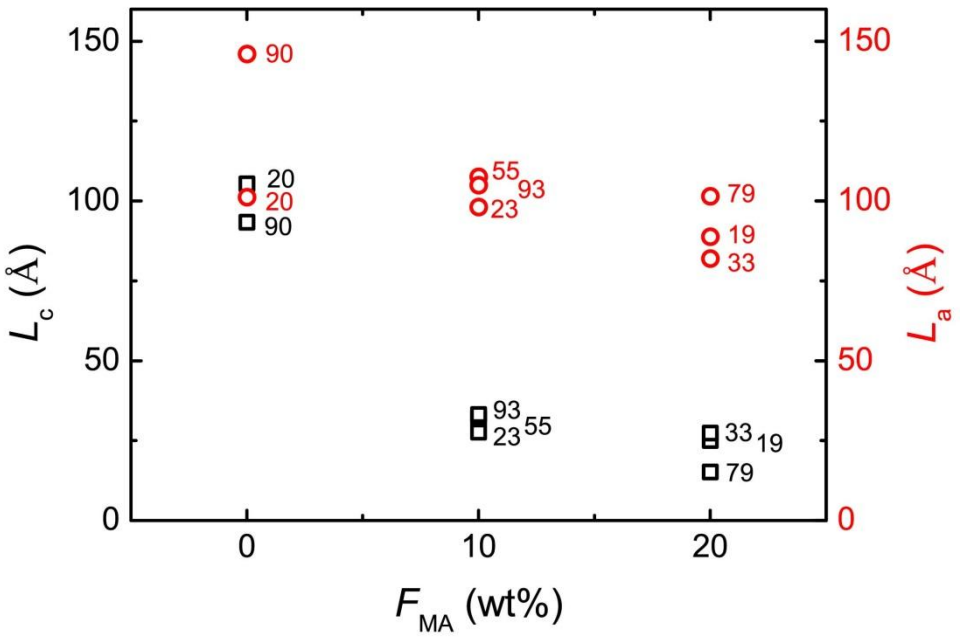

Figure S7 Thickness of lamellae crystal and amorphous domain of p(E-*s*-MA) measured by SAXS and DSC. Number next to symbol denotes the M_n of the copolymer.

The thickness of the crystalline lamellae and the amorphous domain was calculated with long spacing of the lamellae measured from SAXS and crystallinity measured from DSC.

$$L_c = L * X \tag{5}$$

$$L_a = L * (1 - X) \tag{6}$$

L_c is the thickness of crystalline lamellae, L is the long spacing of the lamellae stacking, X is the crystallinity determined from DSC and L_a is the thickness of the amorphous domain.[2]

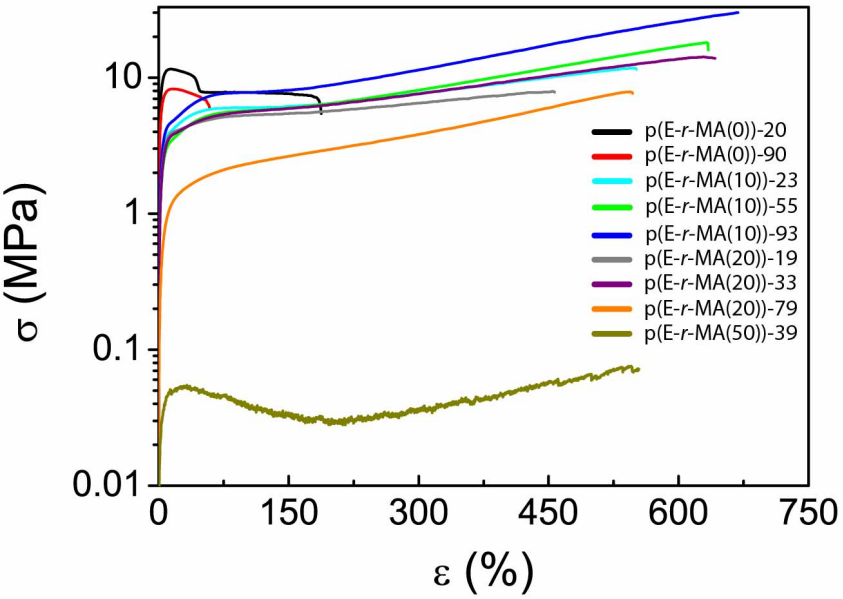

Figure S8. Stress-strain curves of quenched p(E-*s*-MA) series from tensile testing conforming to ASTM D1708 standards. The dog-bone samples were strained at a rate of 5 mm/min. Depending on the MA content, the copolymer exhibits mechanical properties ranging from thermoplastics response to elastomeric behavior.

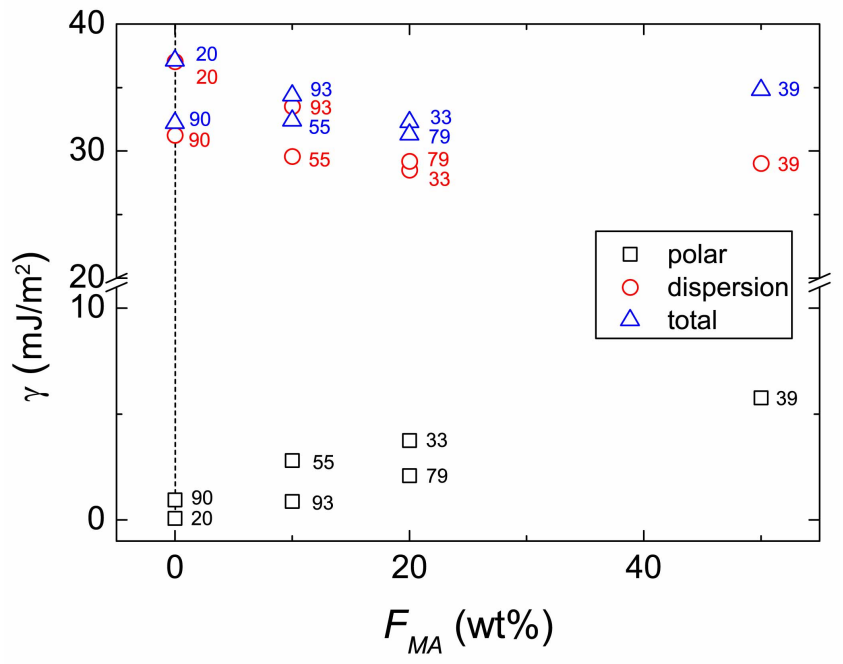

Figure S9. Surface energy of p(E-*s*-MA) from contact angle measurement conforming to ASTM D7490-13. The polar component of the surface tension increases with increasing polar MA co-monomer content while the dispersion component decreases. Total surface energy given by adding polar and dispersion component stays nearly constant around 35 dyn/cm. The number next to the symbol denotes the M_n of the copolymer.

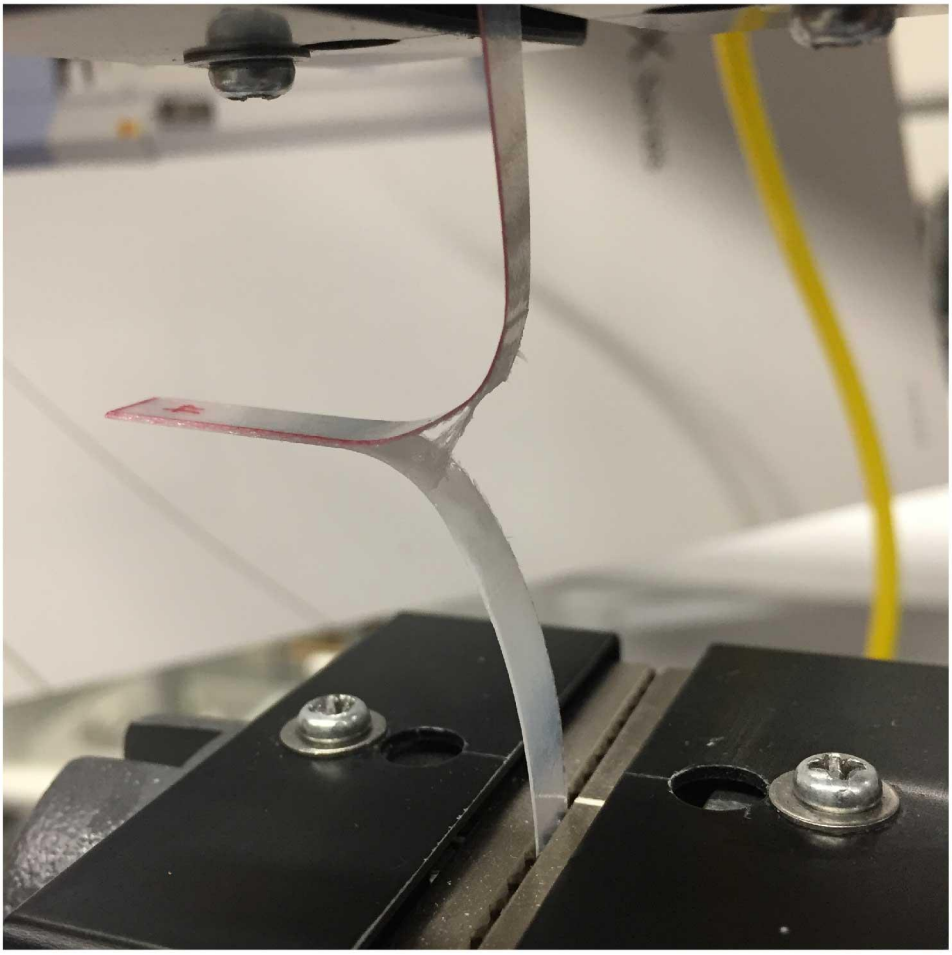

Figure S10. Pictures of PET/p(E-*s*-MA)/PET during T-peel testing.

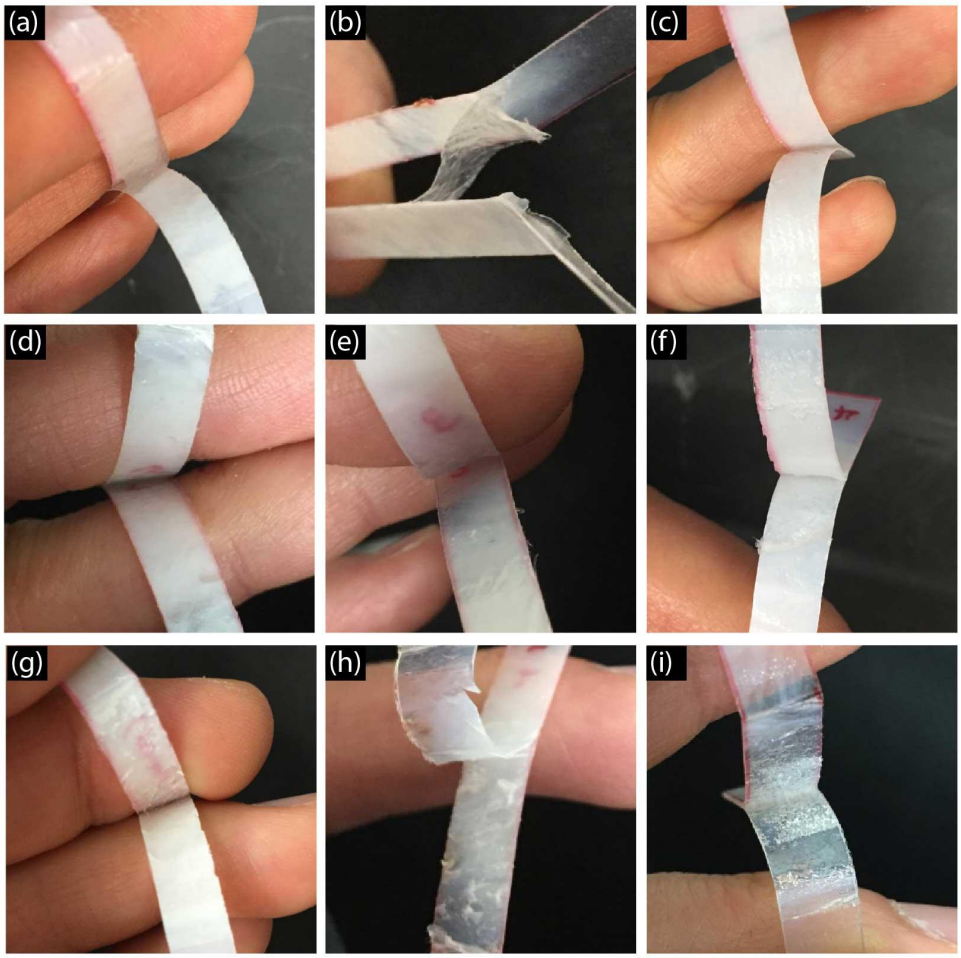

Figure S11. Pictures of laminates of (a) PET/p(E-*s*-MA(0))-20/PET (b) PET/p(E-*s*-MA(0))-90/PET (c) PET/p(E-*s*-MA(10))-23/PET (d) PET/p(E-*s*-MA(10))-55/PET (e) PET/p(E-*s*-MA(10))-93/PET (f) PET/p(E-*s*-MA(20))-19/PET (g) PET/p(E-*s*-MA(20))-33/PET (h) PET/p(E-*s*-MA(20))-79/PET and (i) PET/p(E-*s*-MA(50))-59/PET after peel testing.

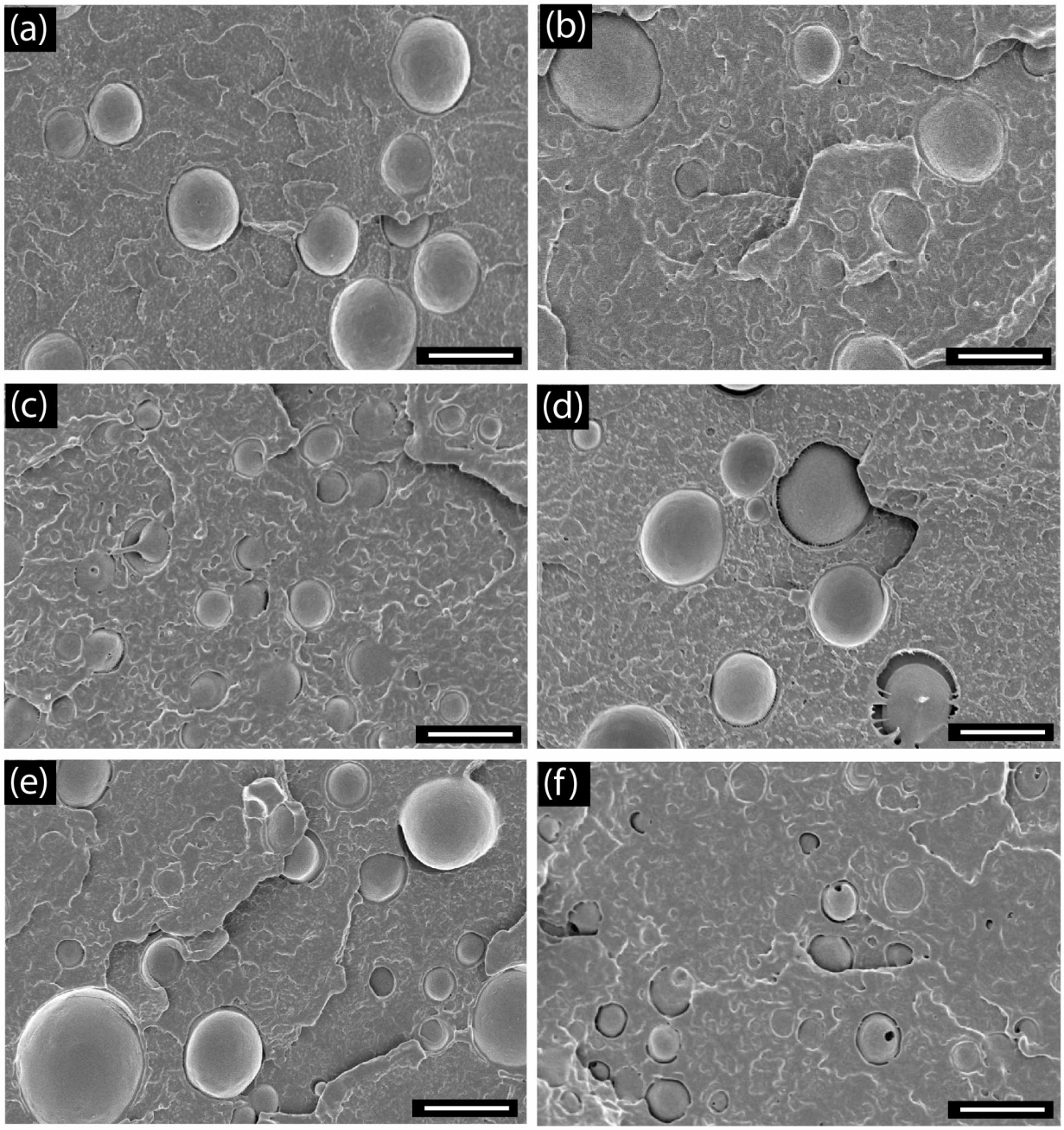
(a)
(b)
(c)
(d)
(e)
(f)

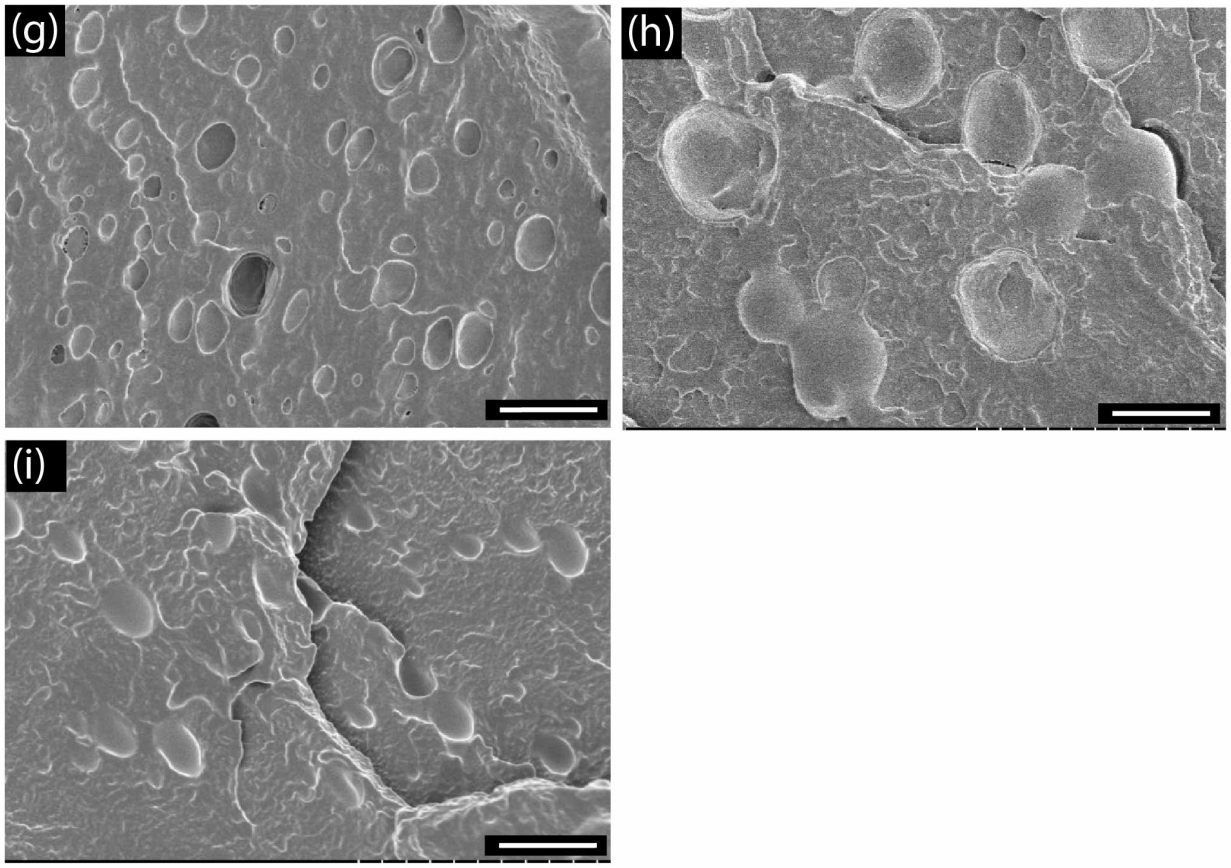

Figure S12. Scanning electron microscope images of (a) PET/p(E-*s*-MA(0))-20 (b) PET/p(E-*s*-MA(0))-90 (c) PET/p(E-*s*-MA(10))-23 (d) PET/p(E-*s*-MA(10))-55 (e) PET/p(E-*s*-MA(10))-93 (f) PET/p(E-*s*-MA(20))-19 (g) PET/p(E-*s*-MA(20))-33 (h) PET/p(E-*s*-MA(20))-79 and (i) PET/p(E-*s*-MA(50))-59. The scale bar denotes 2μm.

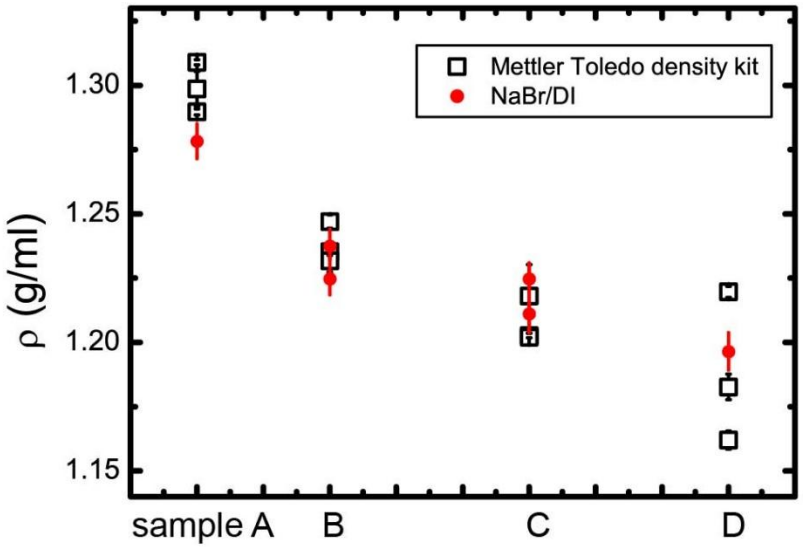

Figure S13. The comparison of the density measured by Metter Toledo XPE205 with density measurement kit and NaBr/DI solution. The values are very similar except slight deviation at around 1.28 g/ml.

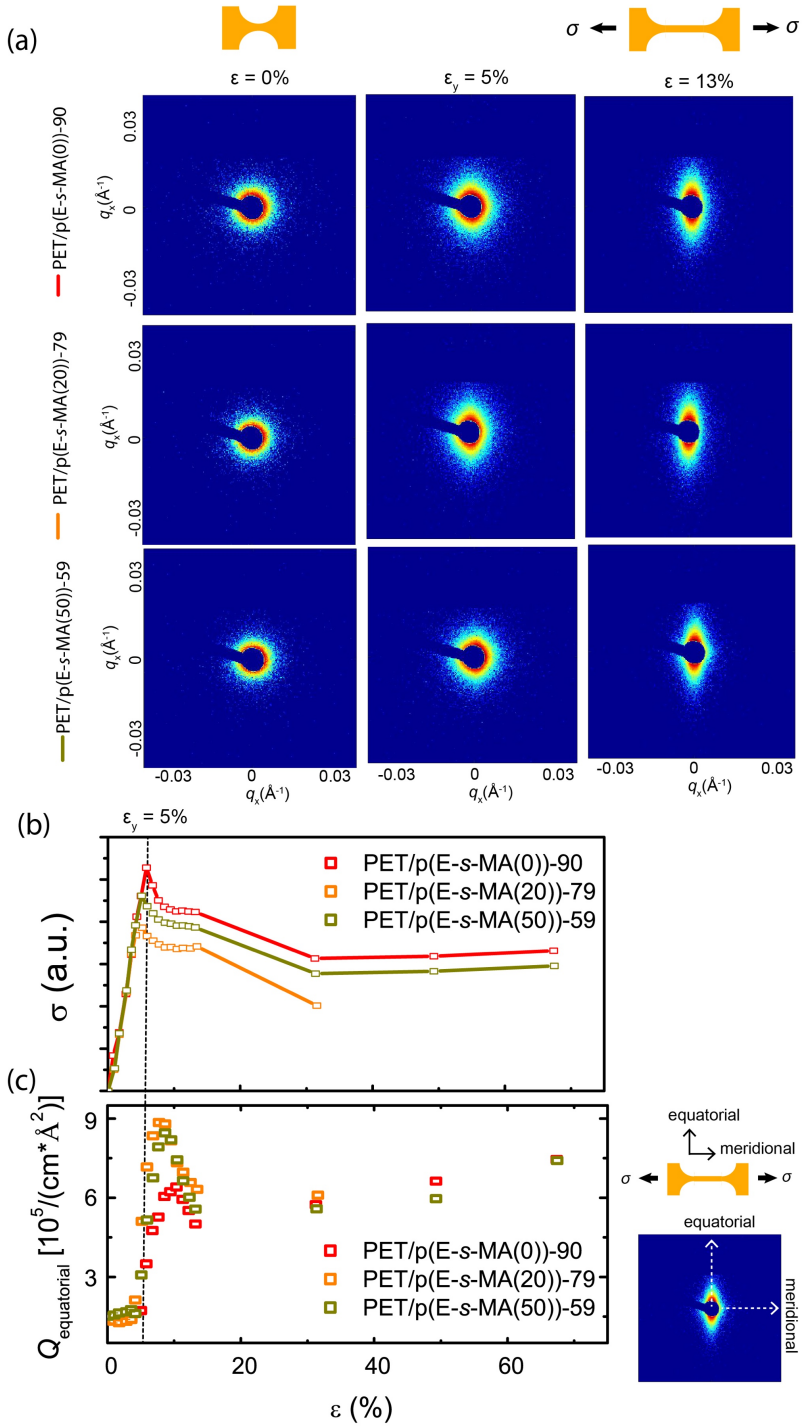

Figure S14. (a) 2D SAXS data and (b) stress-strain curves obtained during in-situ tensile SAXS measurement of PET/p(E-*s*-MA(0))-90, PET/p(E-*s*-MA(20))-79 and PET/p(E-*s*-MA(50))-59. (c) Scattering invariant (Q) in equatorial direction is plotted during in-situ tensile SAXS measurement as a function of strain. Scattering invariant (Q) is calculated as $Q = \frac{1}{2\pi}\int_0^\infty I(q)q^2dq = \phi(1-\phi)(\rho_1-\rho_2)^2$, where ρ_1, ρ_2 are the scattering length density of two phases and ϕ is the volume fraction of the one of the phases. At the yield point , Q increases due to the increased scattering length density contrast between the void (either by cavitation or debonding) and the polymer.

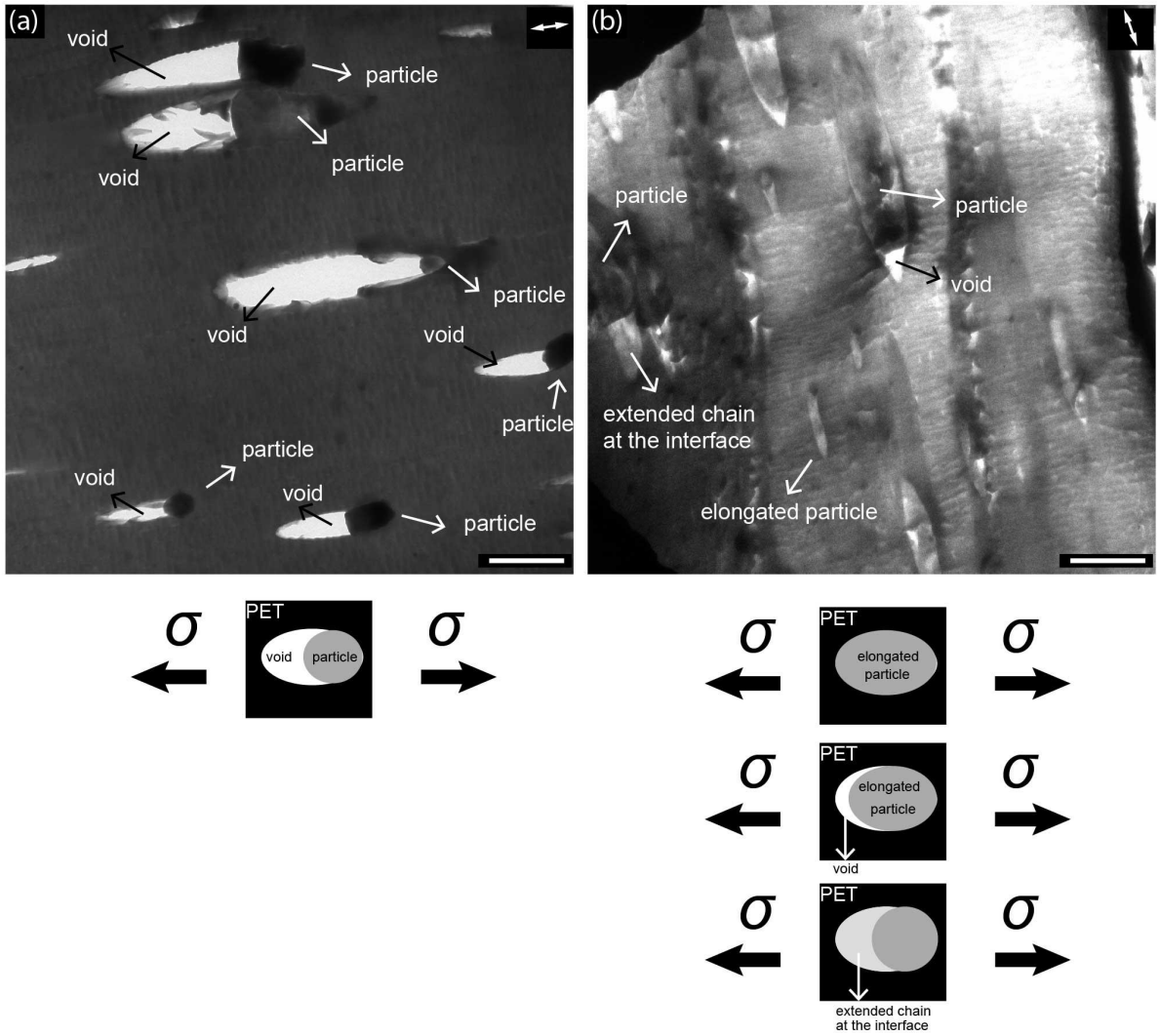

Figure S15. Transmission electron microscopy images of (a) PET/p(E-*s*-MA(0))-20 (b) PET/p(E-*s*-MA(0))-90 to 50-60%. The strain rates were at a 5 mm/min and the arrow denotes the direction of tensile strain. The scale bar denotes 2 μm. The cartoons below the TEM images illustrate the various micro-mechanical deformation behavior observed from each sample.

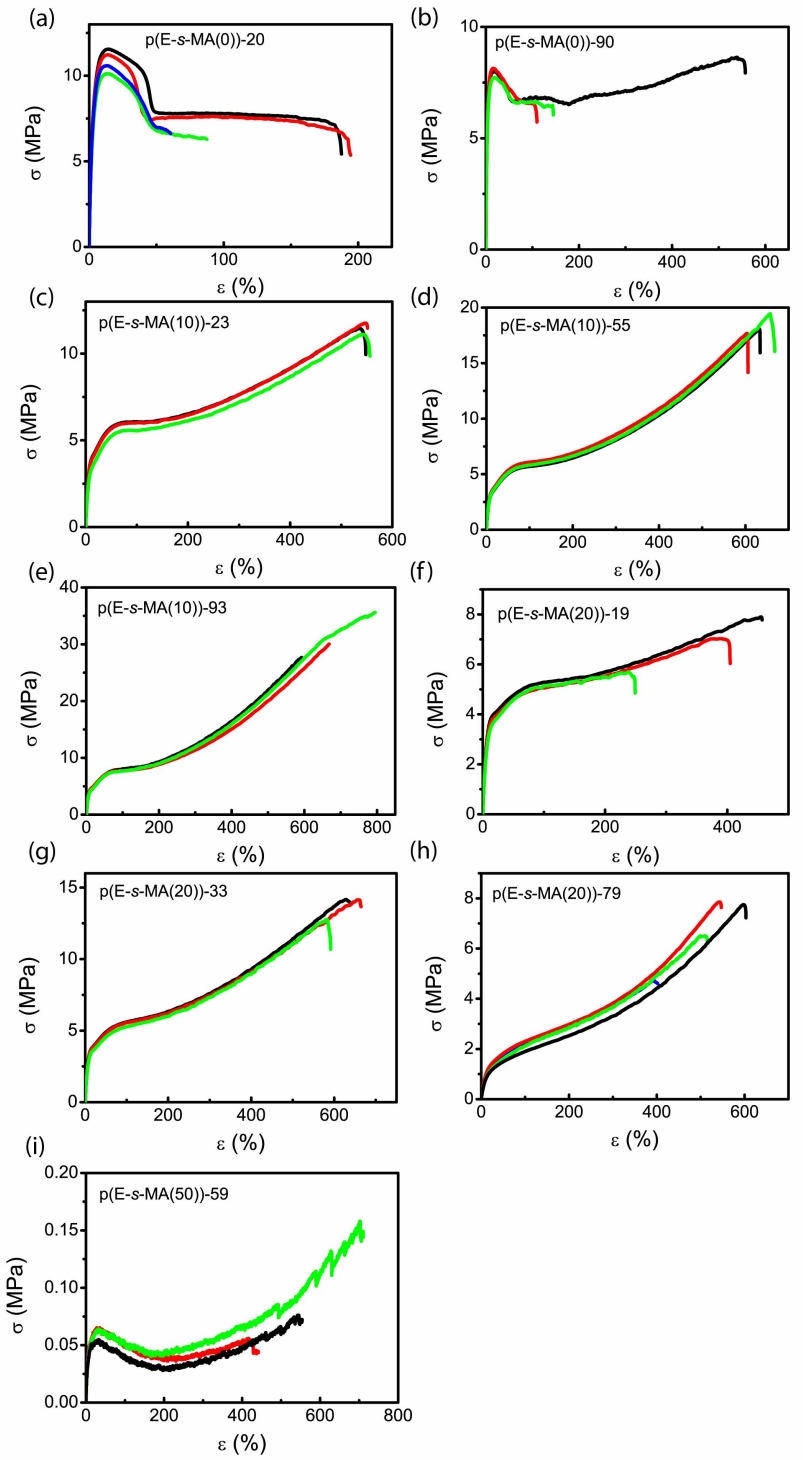

Figure S16. Full list of stress-strain curves of quenched (a) p(E-*s*-MA(0)-20, (b) p(E-*s*-MA(0)-90, (c) p(E-*s*-MA(10)-23, (d) p(E-*s*-MA(10)-55, (e) p(E-*s*-MA(10)-93, (f) p(E-*s*-MA(20)-19, (g) p(E-*s*-MA(20)-33, (h) p(E-*s*-MA(20)-79 and (i) p(E-*s*-MA(20)-59 taken at room temperature. The tensile tests were conducted on Shimadzu Autograph AGS-X tensile tester and the dog-bone samples were strained at a rate of 5mm/min.

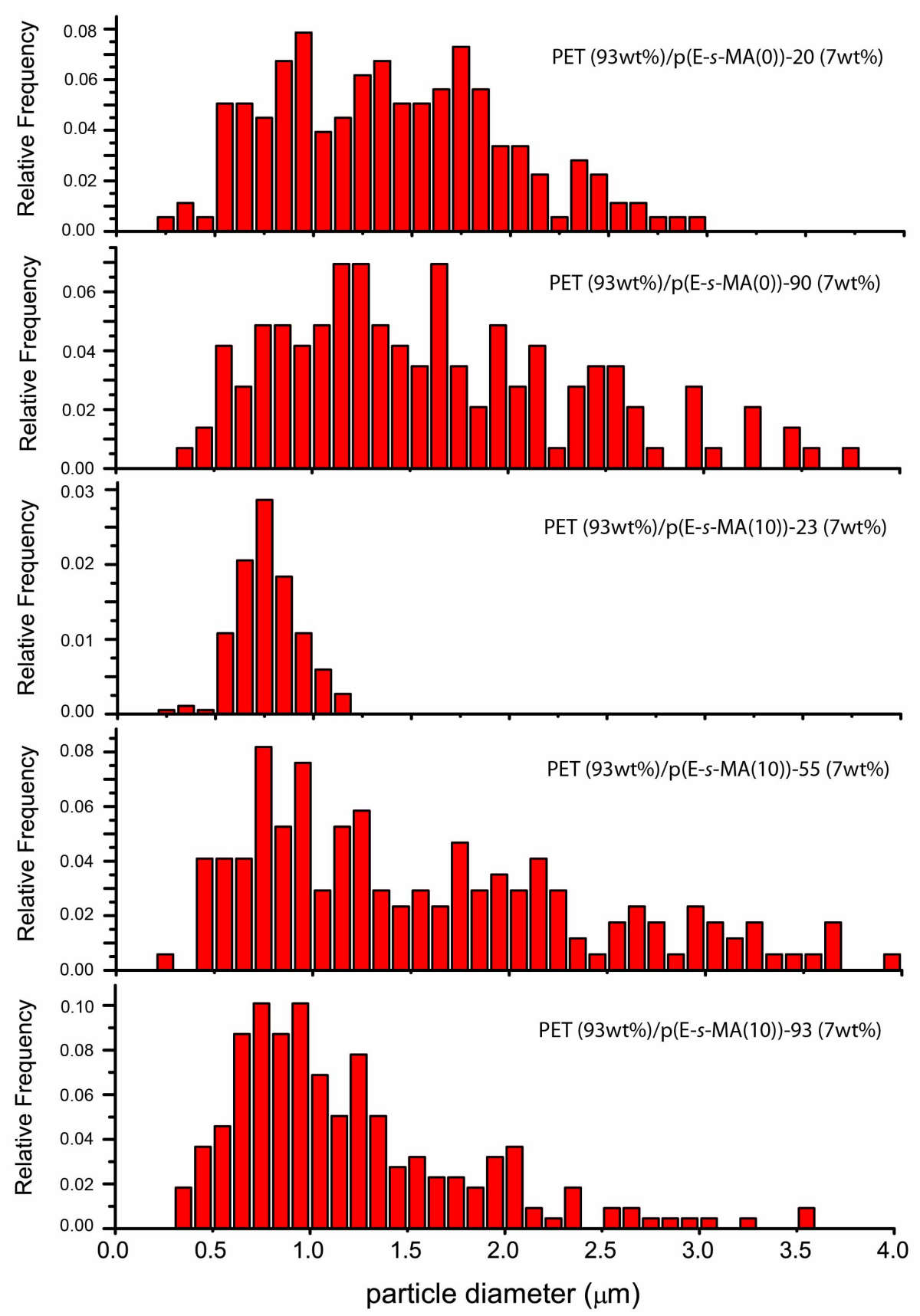
Relative Frequency
PET (93wt%)/p(E-s-MA(0))-20 (7wt%)
PET (93wt%)/p(E-s-MA(0))-90 (7wt%)
PET (93wt%)/p(E-s-MA(10))-23 (7wt%)
PET (93wt%)/p(E-s-MA(10))-55 (7wt%)
PET (93wt%)/p(E-s-MA(10))-93 (7wt%)
0.0
0.5
1.0
1.5
2.0
2.5
3.0
3.5
4.0
particle diameter (μm)

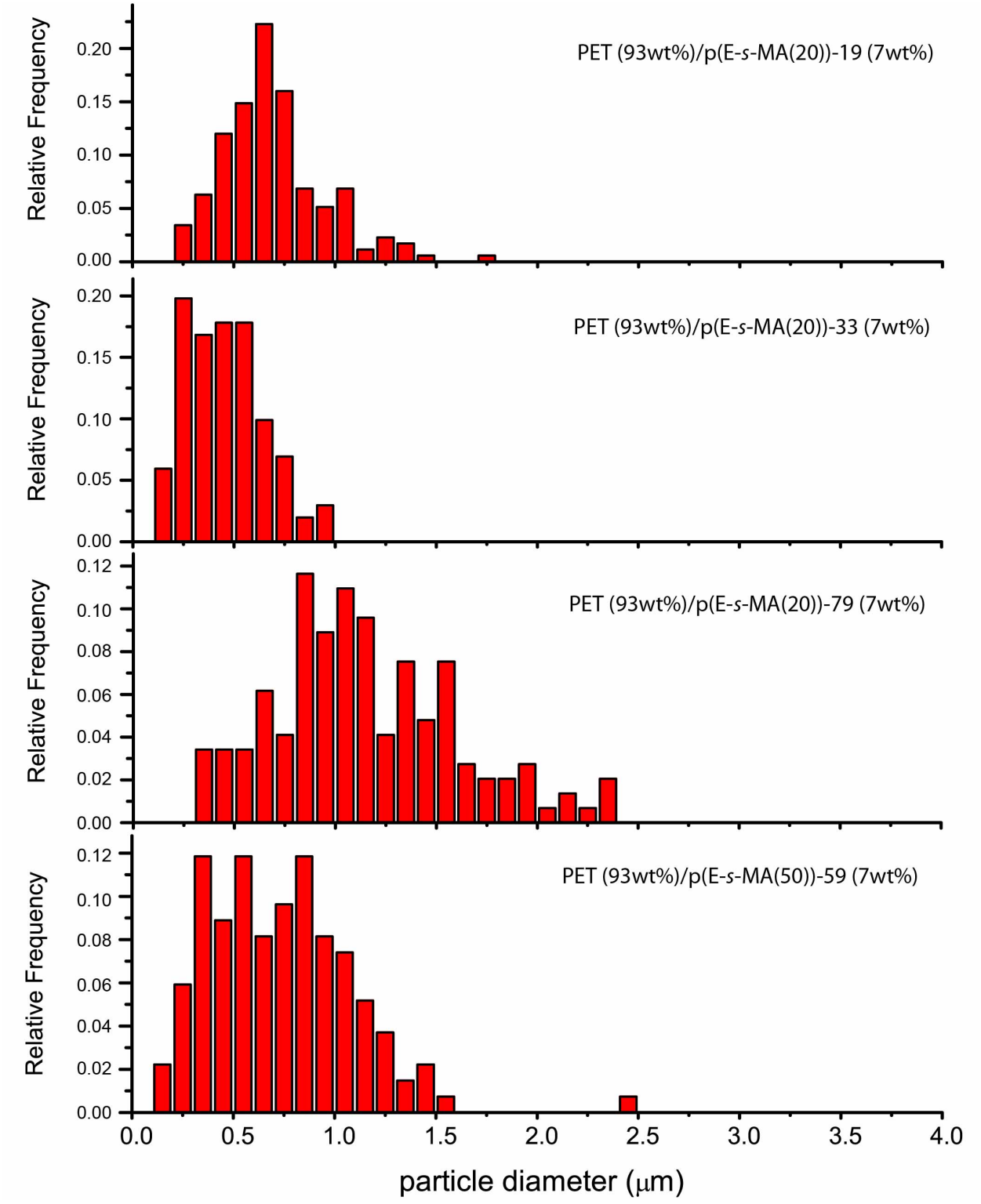

Figure S17. Particle size distribution of PET(93wt%)/p(E-*s*-MA)(7wt%) blends determined from SEM images. The number of particles counted for each blends were between 100 and 220.

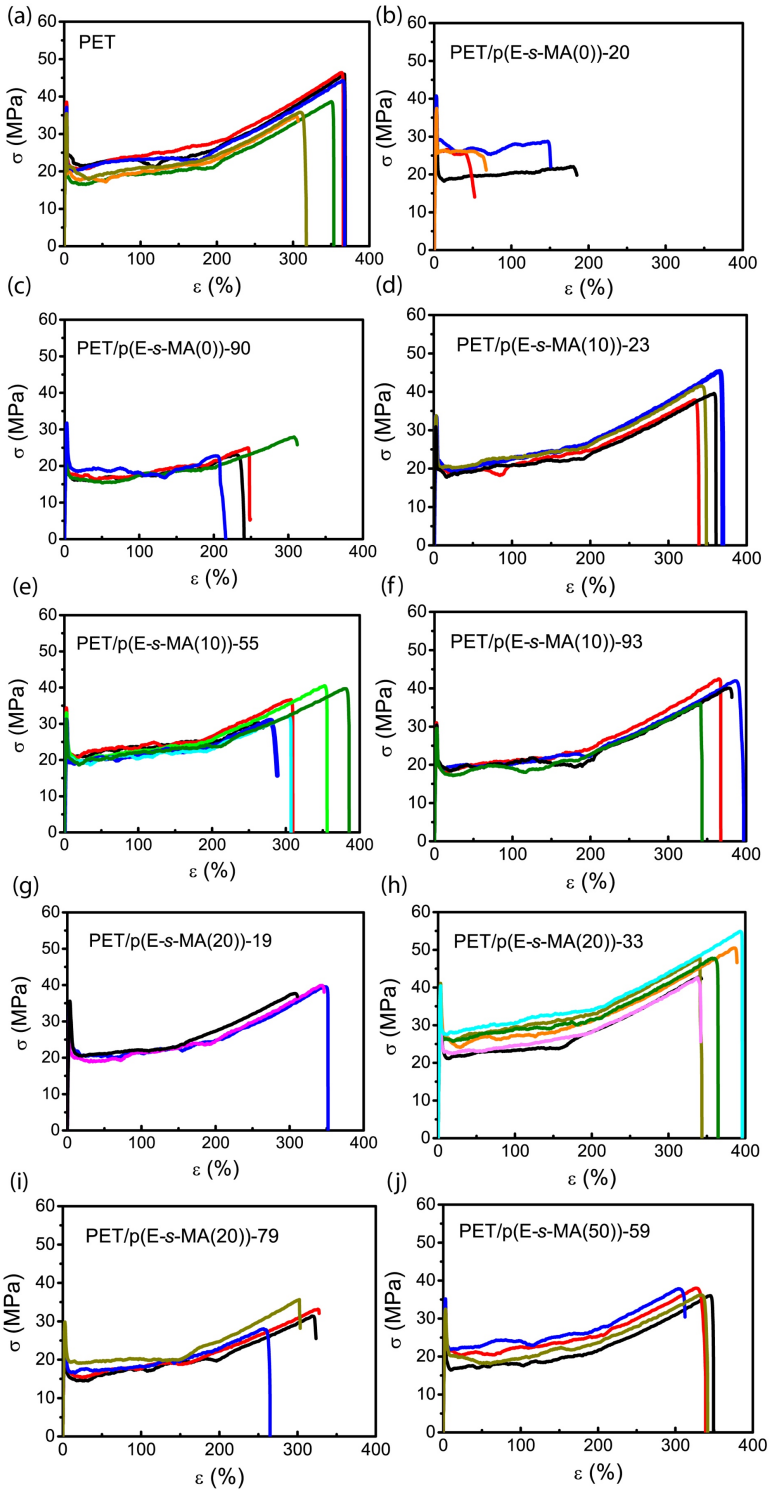

Figure S18. Full list of stress-strain curves of quenched (a) PET (b) PET/p(E-*s*-MA(0)-20, (c) PET/p(E-*s*-MA(0)-90, (d) PET/p(E-*s*-MA(10)-23, (e) PET/p(E-*s*-MA(10)-55, (f) PET/p(E-*s*-MA(10)-93, (g) PET/p(E-*s*-MA(20)-19, (h) PET/p(E-*s*-MA(20)-33, (i) PET/p(E-*s*-MA(20)-79 and (j) PET/p(E-*s*-MA(50)-59 taken at room temperature. The tensile tests were conducted on Shimadzu Autograph AGS-X tensile tester and the dog-bone samples were strained at a rate of 5mm/min.

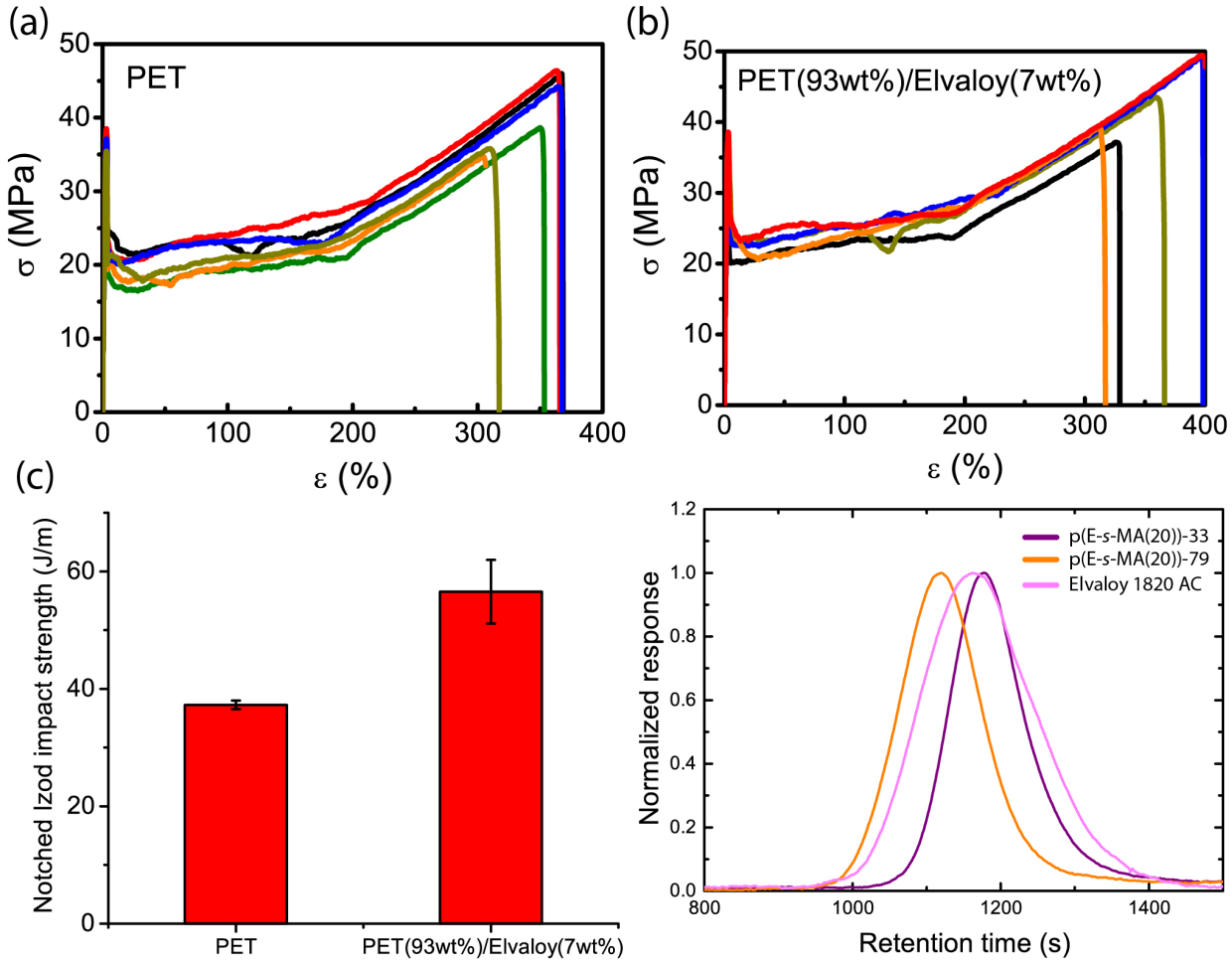

Figure S19. Stress-strain curves of quenched (a) PET (b) PET(93wt%)/Elvaloy 1820AC(7wt%) blend. Elvaloy 1820AC is a copolymer of ethylene and methyl acrylate with 20wt% in methyl acrylate comonomer content. (d) SEC traces of Elvaloy 1820 AC along with synthesized p(E-*s*-MA) copolymers measured at 135 °C with 1,2,4-trichlorobenzene as the eluent at a flow rate of 1.0 mL min^{-1}. The SEC traces are measured by Polymer Laboratories GPC-220 liquid chromatograph fitted with three or two PlGel 10 μm Mixed-B columns and equipped with a refractometer.

Table S1. Mechanical characteristics for the PET and PET/Elvaloy 1820AC blend

Copolymer	E^a (GPa)	$\sigma_y{}^b$ (MPa)	$\sigma_p{}^c$ (MPa)	$\varepsilon_b{}^d$ (%)	Tensile toughness[e] (MJ/m^3)	Notched Izod impact strength[f] (J/m)
PET	1.73±0.04	35.6±2.6	23.3±7.8	344±31	92±18	37±1
PET(93wt%)/ Elvaloy1820AC(7wt%)	1.66±0.04	36.2±3.3	23.4±2.0	359±43	106±21	57±5

[a]Elastic modulus; measured from the linear proportion of the stress-strain curve (initial 1%).

[b]Yield stress. [c]Plateau stress. [d]Elongation at break. [e]Tensile toughness was determined by integrating the stress-strain curve to the point of break. [f]Notched Izod impact strength samples conforming to ASTM D256 standard were prepared by Morgan Press injection molder and notched with a CEAST NotchVis notcher. Izod Notched Izod impact strength was measured by CEAST impact strength tester (model 6545). All specimens were aged in room temperature for two days before test. At least 4-5 specimens were tested for each sample to obtain statistically significant data.

Table S2. Comparison of characterization data for Elvaloy 1820AC and p(E-*s*-MA) with F_{MA}=20wt%

Name	F_{MA} (wt%)	M_n (kDa)[a]	$Đ$	T_m (°C)[b]	$T_{d,5\%}$ (°C)[c]	X (%)[d]
Elvaloy 1820 AC	20	24	5.3	92	329	18
p(E-*s*-MA(20))-19	20	19	2.5	91	306	22
p(E-*s*-MA(20))-33	20	33	2.2	89	329	25
p(E-*s*-MA(20))-79	20	79	2.8	83	351	13

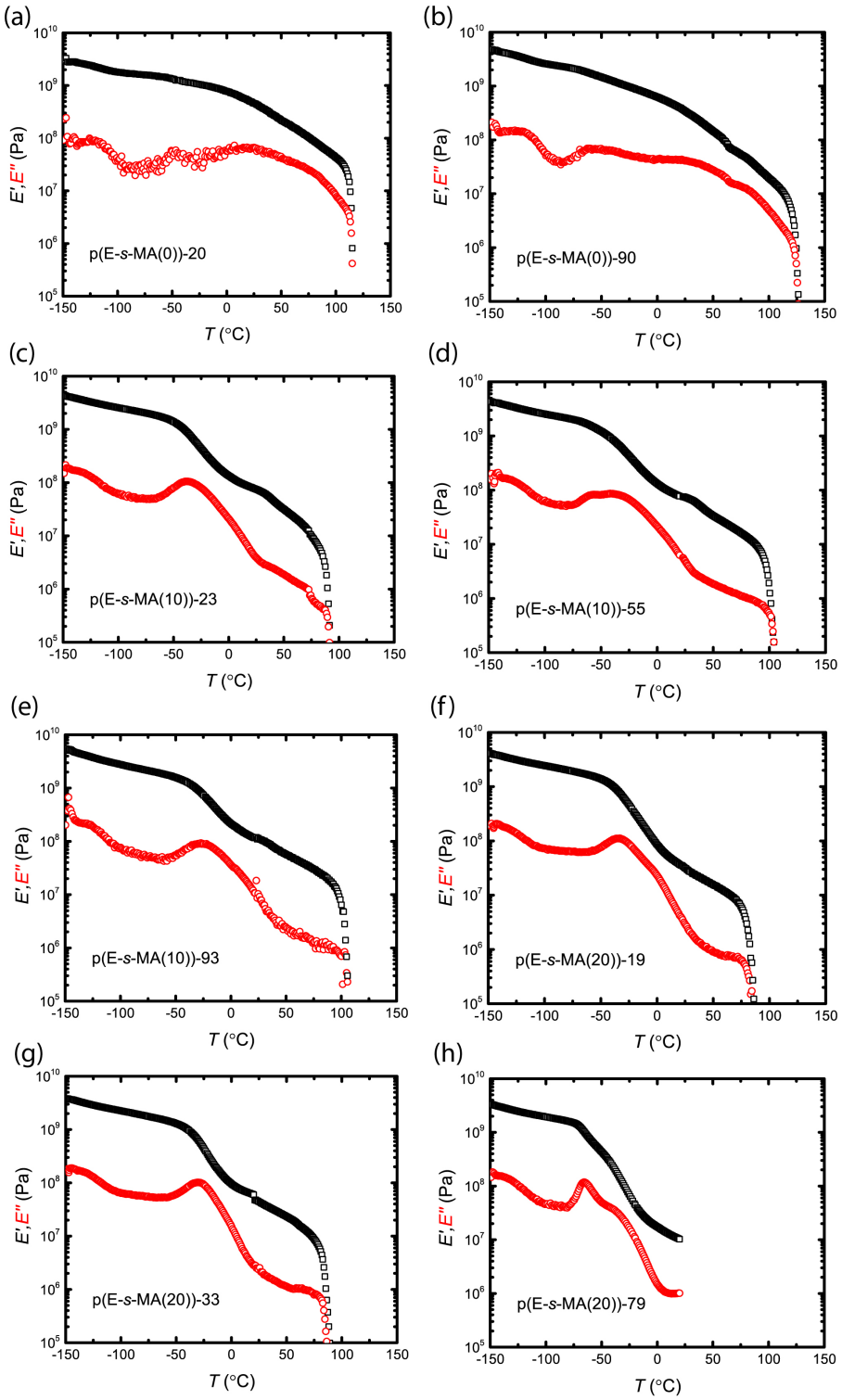

Figure S20. DMTA curves showing storage modulus (black) and loss modulus (red) of (a) p(E-*s*-MA(0)-20, (b) p(E-*s*-MA(0)-90, (c) p(E-*s*-MA(10)-23, (d) p(E-*s*-MA(10)-55, (e) p(E-*s*-MA(10)-93, (f) p(E-*s*-MA(20)-19, (g) p(E-*s*-MA(20)-33 and (h) p(E-*s*-MA(20)-79. TA instrument RSA-G2 was used to measure DMTA and ramping rate was 5°C/min. The glass transition temperature of each copolymer was determined from the peak of loss modulus.

Table S3. Comparison of glass transition temperatures determined from DSC and DMA.

Name	$T_{g,DSC}$[a] (°C)	$T_{g,DMA}$[b] (°C)
p(E-*s*-MA(0))-20	Not determined	−120
p(E-*s*-MA(0))-90	Not determined	−119
p(E-*s*-MA(10))-23	−37	−36
p(E-*s*-MA(10))-55	Not determined	−34
p(E-*s*-MA(10))-93	−26	−26
p(E-*s*-MA(20))-19	−29	−33
p(E-*s*-MA(20))-33	−30	−30
p(E-*s*-MA(20))-79	−65	−65
p(E-*s*-MA(50))-59	−43	

[a]Glass transition temperature was determined from 2nd heating of the DSC measurement at a ramping rate of 10 °C/min. [b]Glass transition temperature was determined from the peak of loss modulus via DMTA measurement at a ramping rate of 5 °C/min.

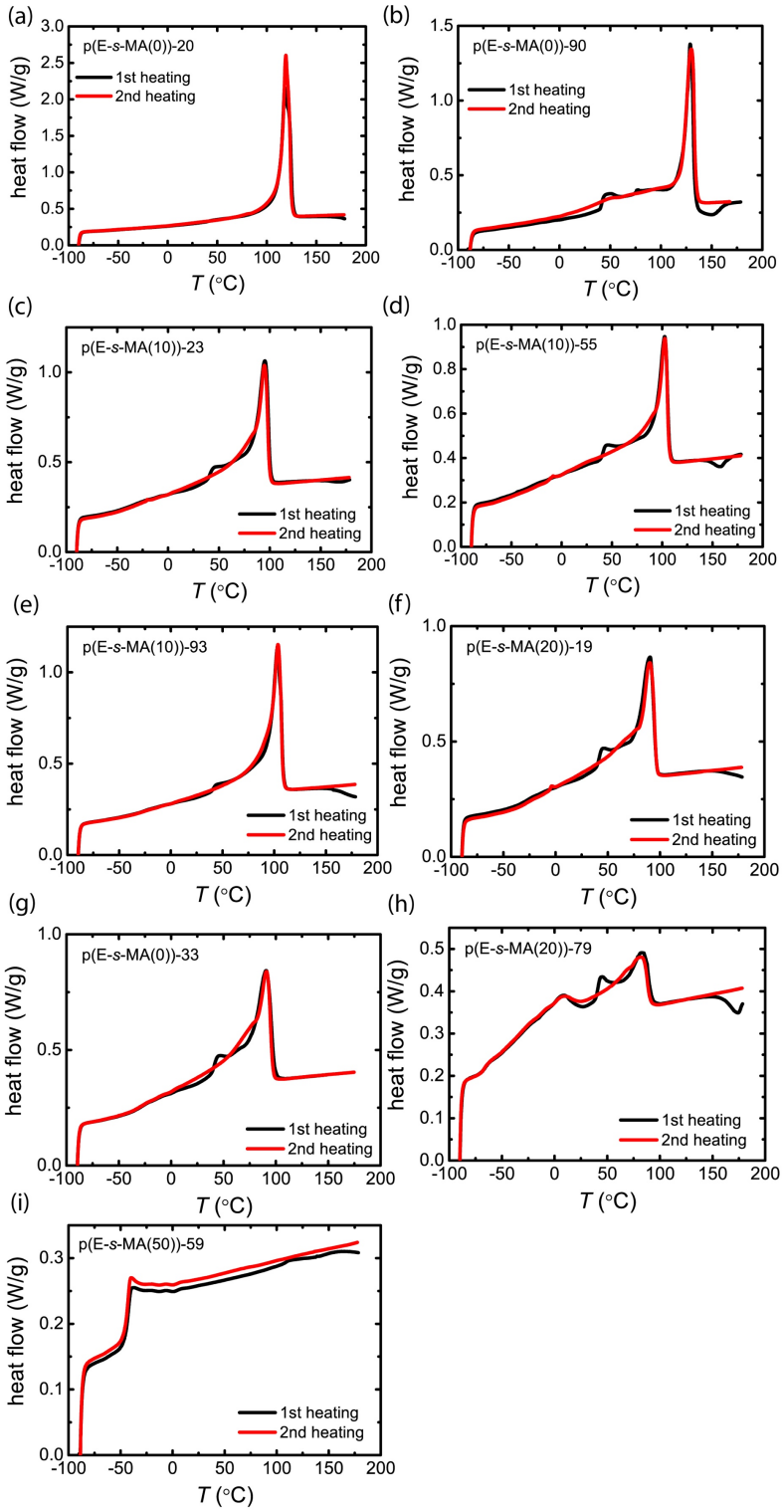

Figure S21. DSC curves of quenched (a) PET/p(E-*s*-MA(0)-20, (b) PET/p(E-*s*-MA(0)-90, (c) PET/p(E-*s*-MA(10)-23, (d) PET/p(E-*s*-MA(10)-55, (e) PET/p(E-*s*-MA(10)-93, (f) PET/p(E-*s*-MA(20)-19, (g) PET/p(E-*s*-MA(20)-33, (h) PET/p(E-*s*-MA(20)-79 and (i) PET/p(E-*s*-MA(20)-59 during 1st and 2nd heating ramp at a rate of 10 °C/min. Samples were hot pressed at 180 °C and quenched on a cold water-jacketed press.

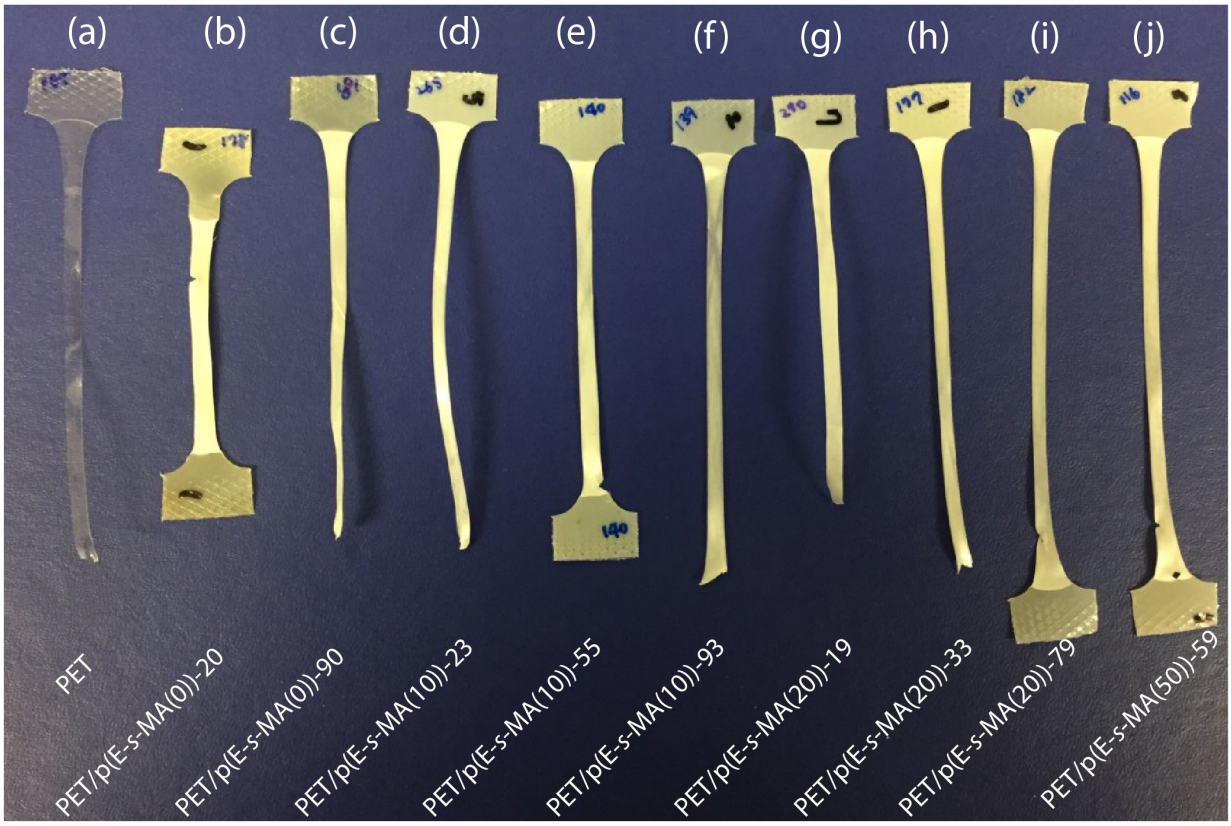

Figure S22. Picture of strained tensile bars of (a) PET (b) PET/p(E-*s*-MA(0)-20, (c) PET/p(E-*s*-MA(0)-90, (d) PET/p(E-*s*-MA(10)-23, (e) PET/p(E-*s*-MA(10)-55, (f) PET/p(E-*s*-MA(10)-93, (g) PET/p(E-*s*-MA(20)-19, (h) PET/p(E-*s*-MA(20)-33, (i) PET/p(E-*s*-MA(20)-79 and (j) PET/p(E-*s*-MA(50)-59. Whitening of the gauge area supports our explanation that voids are formed during tensile deformation by either cavitation or de-bonding for most of PET/p(E-*s*-MA) blends.

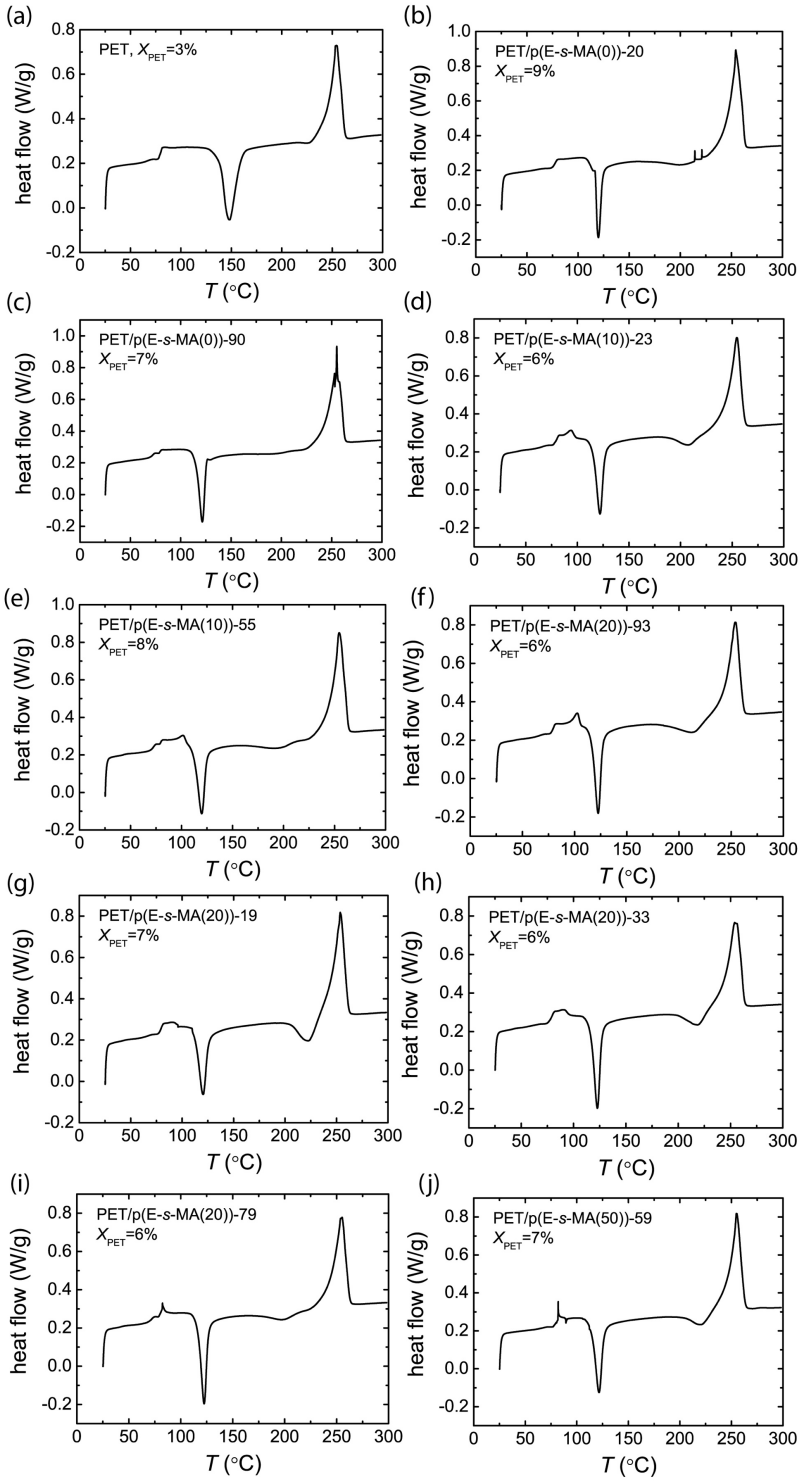

Figure S23. DSC curves of quenched tensile bars of (a) PET (b) PET/p(E-*s*-MA(0)-20, (c) PET/p(E-*s*-MA(0)-90, (d) PET/p(E-*s*-MA(10)-23, (e) PET/p(E-*s*-MA(10)-55, (f) PET/p(E-*s*-MA(10)-93, (g) PET/p(E-*s*-MA(20)-19, (h) PET/p(E-*s*-MA(20)-33, (i) PET/p(E-*s*-MA(20)-79 and (j) PET/p(E-*s*-MA(50)-59 during 1st heating at a ramping rate of 10 °C/min.

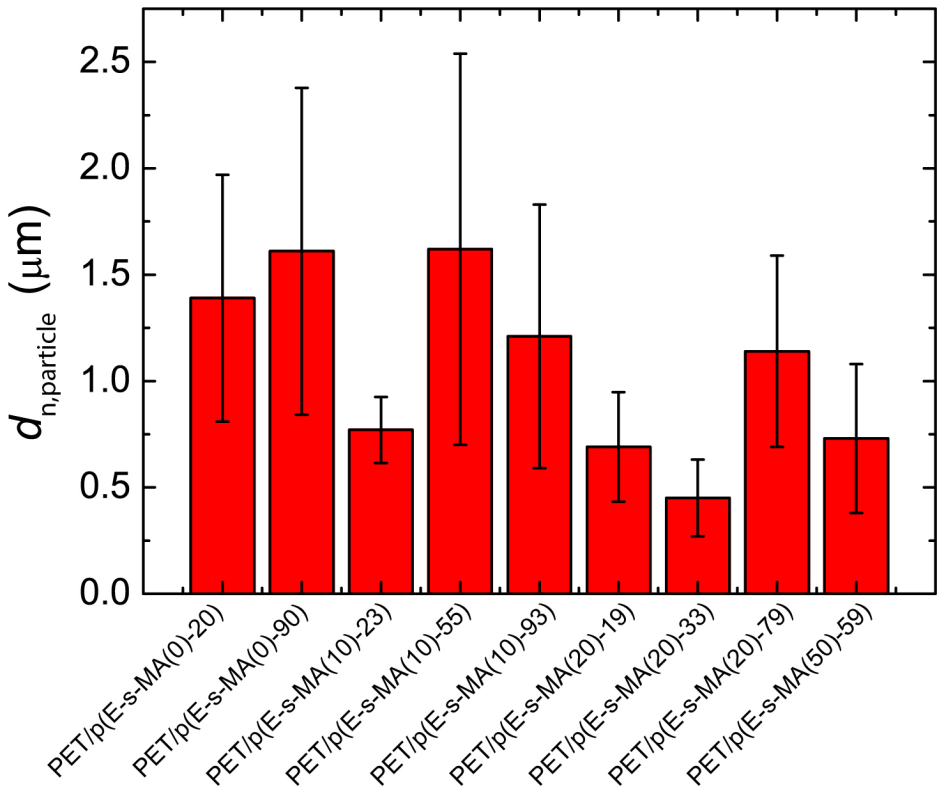

Figure S24. The number average particle diameters of PET(93wt%)/p(E-*s*-MA)(7wt%) were measured from the SEM images. The error bars denote the standard deviation from measurements of 160 particles (on average) for each blend

Reference

(1) Huang, Y.-L.; Brown, N. Dependence of Slow Crack Growth in Polyethylene on Butyl Branch Density: Morphology and Theory. *J. Polym. Sci. Part B-Polymer Phys.* **1991**, *29*, 129–137.

(2) Hosoda, S.; Nozue, Y.; Kawashima, Y.; Utsumi, S.; Nagamatsu, T.; Wagener, K.; Berda, E.; Rojas, G.; Baughman, T.; Leonard, J. Perfectly Controlled Lamella Thickness and Thickness Distribution: A Morphological Study on ADMET Polyolefins. *Macromol. Symp.* **2009**, *282* (1), 50–64.